Journal of Nonlinear Mathematical Physics (2025) 32:59
https://doi.org/10.1007/s44198-025-00316-2

RESEARCH

Dynamics of the Forced Thirring Instanton with Two Forcing Terms

Mine Ak[1]

Received: 7 February 2025 / Accepted: 11 August 2025

Abstract

We consider the dynamical behavior of fermionic instanton solutions of the Thirring Model with two forcing terms. In particular, the study focuses on the effect of the frequency and amplitude of the forcing terms on the behavior of fermionic instanton solutions. Numerical analysis based on the Smaller Alignment Index (SALI) method, Bifurcation Diagram and Permutation Entropy (PE) are used to show how and which dynamical behaviors occur in the system. Color maps and diagrams of the SALI time (S_t) (the time S_t required for the SALI index to below a threshold value of 10^{-12}) and PE of the system with respect to varying of frequency and amplitude values of the forcing terms are plotted comparatively to determine different dynamical behavior of the system. The study shows that fermionic instanton solutions exhibit a wide variety of dynamical behavior due to two forcing terms. Furthermore, it is emphasized that SALI time (S_t) can be easily compared with bifurcation diagram and complexity method as a fast, efficient and precise method to investigate different degrees of chaos. In general, the instanton solutions with two forcing terms have been observed to exhibit different type of dynamical behavior. In this study, identical and symmetric coexisting attractors are demonstrated for these different types of behavior of the forced Thirring instanton.

Keywords Nonlinear dynamical systems · Instanton · Chaos · Smaller alignment index (SALI) method, permutation entropy

✉ Mine Ak
mine.ak@istun.edu.tr

[1] Department of Mechatronics Engineering, Faculty of Engineering and Natural Sciences, Istanbul Health and Technology University, Istanbul, Turkey

Published online: 28 August 2025

1 Introduction

Instantons are topological objects in quantum field theory that are related to tunneling transitions between two distinct vacuum states [1]. They are interpreted as a quantum tunneling effect, in which a fermion is able to tunnel through a barrier of energy. This process, known as quantum tunneling, is a quantum mechanical phenomenon in which particles can pass through barriers of energy that would otherwise be impassable [2]. They are used to study the behavior of fermionic systems, the effects of interactions between particles, and the effects of quantum fluctuations [3]. In quantum field theory, instantons are important because they are the only known way to generate a non-zero and finite action solutions. This means that they can be used to describe a wide range of physical phenomena, such as particle creation, tunneling, and other effects [4–9]. Moreover, instantons are used to describe the strong interaction between quarks and gluons in the standard model of particle physics and how particles interact with curved spacetime, such as black holes and cosmological horizons [10–12]. Since instantons are responsible for spontaneous symmetry breaking in certain theories, they allow particles to behave differently under different conditions and can be thought of as responsible for much of the complexity in the universe.

The massless Thirring model [13] is a quantum field theory that describes a system of interacting fermions in one space and one-time dimensions. It was proposed by Walter Thirring in 1958 and has since been the subject of extensive study in theoretical and mathematical physics [14–16]. The Lagrangian of the Thirring model [13], which in space-time $(1+1)$ dimensions defines a Fermi self-interaction, with positive coupling constant g, for fermion field with spin ½ is

$$L = i\,\bar{\psi}\;\sigma_{\mu}\,\partial_{\mu}\,\psi\; + \frac{g}{2}\left(\bar{\psi}\;\psi\right)^{2}, \tag{1}$$

where ψ is fermion, σ_{μ} as $\mu = 1,2$ are Pauli matrices. It has also served as a useful toy model for studying the effects of interactions between fermions. The stable fermionic instanton solutions of the Thirring model were found [17]. Then, a nonlinear system of ordinary differential equations corresponding to the fermionic instanton solutions in the Thirring field equation was obtained via Heisenberg ansatz [18]. The evolution of these solutions according to the coupling constant was investigated in the phase space in Ref [18] and also implemented in the Gursey model [19]. Then, the stability of the instanton solutions was analyzed by the Scale Index Method [20]. Recently, the chaotic nature of fermionic instanton solutions under a single force has been investigated using the Generalized Alignment Index of order 2 ($GALI_2$) and largest Lyapunov exponent (LLE) methods comparatively [21]. And the Thirring model has been used to investigate chaos and complexity in the evolution of the universe [22, 23].

Dynamical systems that exhibit a variety of behaviors, some regular, some chaotic, and some both regular and chaotic, are studied using mathematical models and simulations [24]. Dynamical systems are characterized by their sensitivity to initial conditions; this means that small changes in initial conditions can have large effects on the behavior of the system over time. Chaos theory is the study of chaotic behavior in dynamical systems. This sensitivity can cause a dynamic system to go from a

normal state to a chaotic state in a very short time, while its occurrence over a longer period of time can cause it to go into a weakly chaotic state [25].

Hamiltonian systems encounter difficulties in distinguishing the nature of the orbits, which are unpredictably distributed in phase space. Therefore, a fast and precise calculation is essential for detecting the regular or chaotic state of the orbit. The Smaller Alignment Index (SALI) method is an effective method that fulfills these requirements [26, 27]. It should be noted that SALI is practically equivalent to the $GALI_2$ [28]. The SALI method is based on the investigation on the evolution of volume elements formed by deviation vectors with respect to trajectories of a dynamical system [29]. The SALI tends to zero, following the power law for the regular nature of the system, and exponentially for its chaotic nature. Another important detail is that the chaoticity decreases as the time for SALI tending to zero increases. As can be understood from this detail, the time required for the SALI or $GALI_2$ to be zero is an indicator of the chaotic power of the system [21, 29, 30]. In addition, weak chaos refers to systems for which the phase-space dynamics present a mixture of chaotic and regular dynamics, depending on the initial values [31]. In addition, this study aims to show that SALI or $GALI_2$ time method, which is a fast and effective tool for chaos detection, can be compared more easily with other methods such as bifurcation diagram and complexity measures.

In present study, in order to understand how fermionic particles can exhibit behaviors under with forcing, it is investigated how two forcing terms affect the behavior of Thirring instanton in terms of different values of frequency and amplitude. The analysis of numerical study of this research is based on the SALI, Permutation entropy (PE) and bifurcation diagram. The SALI time (S_t) is used to distinguish between different degrees of chaos, as it reveals exactly when chaoticity occurs. Considering both the SALI and PE method results, different degrees of chaos and complexity are observed in terms of the varying frequency and amplitude values of two forcing terms in instanton solutions. Moreover, novel strange attractors corresponding to different type of dynamical behavior are presented in the phase portraits.

The rest of this paper is arranged as follows. In Sect. 2 the model of forced Thirring instanton is presented and numerical methods used to study the dynamics of the model are introduced, namely, the Smaller Alignment Index method, the Bifurcation diagram and the Permutation entropy method. Section 3 presents the results of the study in detail. Finally, Sect. 4 is devoted to the main conclusions.

2 The Model and Numerical Techniques

2.1 The Model

The Heisenberg ansatz according to Euclidean configuration is as follows

$$\psi = [ix_\mu \sigma_\mu \chi(s) + \phi(s)]\, c \tag{2}$$

where $\chi(s)$ and $\varphi(s) \in \mathbb{R}$ ($s = x_1^2 + x_2^2$) and c is defined as an arbitrary constant. Combining The equation of motion for Thirring model with Heisenberg ansatz and con-

verting to a dimensionless form, the nonlinear ordinary differential equation system obtained from the calculations in Ref [18] is presented by,

$$\begin{cases} 2\frac{dp(t)}{dt} + \frac{1}{2}p\,(t) - gAB\left(p(t)^2 + q(t)^2\right)q\,(t)\,c\overline{c} = 0 \\ 2\frac{dq(t)}{dt} - \frac{1}{2}q\,(t) - gAB\left(p(t)^2 + q(t)^2\right)p\,(t)\,c\overline{c} = 0 \end{cases} \tag{3}$$

where A, B are constants, $p(t)$ and $q(t) \in \mathbb{R}$ correspond to dimensionless functions [18]. Here all constants ($gABc\overline{c}$) can be defined as β.

$f_1 \cos(\omega_1 t)$ and $f_2 \cos(\omega_2 t)$, which is considered as external periodic forcing terms, are added to the system (3). These forcing terms can be interpreted as periodic background fields or perturbations acting on fermionic instantons. Obviously, periodic forcings are used to simulate the effects of external time-dependent effects, such as external electromagnetic fields and interactions with a structured background, which may act on the dynamics of the fermionic instanton.

The modified system is given by,

$$\begin{cases} \frac{dp}{dt} = -\frac{1}{4}p + \frac{1}{2}\beta\,\left(p^2 + q^2\right)q + f_1 cos\,(\omega_1 t) \\ \frac{dq}{dt} = \frac{1}{4}q - \frac{1}{2}\beta\,\left(p^2 + q^2\right)p + f_2 cos\,(\omega_2 t) \end{cases} \tag{4}$$

where ω_1 and ω_2 are frequencies, f_1 and f_2 are amplitudes of two forcing terms. β, f_1, f_2, ω_1 and ω_2 are positive. Thanks to the system (4), it is possible to investigate the effect of two forcing terms on the chaotic nature of the fermionic instanton solutions.

2.2 Numerical Techniques

The Smaller Alignment Index (SALI) a fast and effective chaos detection technique, is successfully used to analyze Hamiltonian system behavior [26, 27]. The SALI is determined through the evolution of two initially linearly independent deviation vectors from the initial condition. The deviation vectors are normalized at each time step, since only the trajectory of this vector is considered. At each time step, each vector is normalized to 1 by $\widehat{w}_i\,(t) = \frac{w_i(t)}{||w_i(t)||}$, where $i \in \{1,\ 2\}$ and $||\,.||$ denotes the usual Euclidean norm and define the parallel alignment index

$$d_-\,(t) \equiv\ ||\widehat{w}_1\,(t) - \widehat{w}_2\,(t)\,|| \tag{5}$$

.

and the antiparallel alignment index

$$d_+\,(t) \equiv\ ||\widehat{w}_1\,(t) + \widehat{w}_2\,(t)\,|| \tag{6}$$

.

The smaller alignment index SALI is given by

$$SALI\ \ (t) = min\,\{d_-\,(t)\,,\ d_+\,(t)\} \tag{7}$$

.

The SALI method describes the chaoticity by the exponential decay of the index [26, 27, 30]. If the SALI is practically zero ($<10^{-12}$) until the last time t considered during the integration of the system, the behavior is chaotic; otherwise, the orbit is regular. S_t (SALI time) is the time it takes for *SALI* to reach the threshold value, which indicates chaoticity. If the S_t is a short, behavior is chaotic, if the S_t is a long, behavior is weakly chaotic, and if it does not reach this even for a certain an extremely long time, behavior is regular [21, 28–31]. In this study, diagram and color bar of SALI time (S_t) are calculated by taking the axis symmetry of SALI positive time (i.e. negative time) in order to compare with color maps and diagrams of Permutation entropy and bifurcation diagrams more appropriate.

Bifurcation diagram is an important method for visualizing the behavior of a dynamical system. It shows how the attractors of the system change as the initial conditions and parameters of the system change. In a bifurcation diagram, each point in the diagram represents a different set of parameters, and the attractors correspond to the resulting behavior of the system. It presents critical points at which a system undergoes a qualitative change in behavior, such as the onset of chaos or the emergence of a regular state. It is generally used in chaos studies in comparison with maximum Lyapunov exponential diagrams or Lyapunov exponential spectrums. In this study, it is used in comparison with the SALI/GALI$_2$ time methods, which are similar to the maximum Lyapunov exponents. In this way, a fast and effective alternative comparison method in chaos research is aimed.

In general, complexity is a measure of the randomness of a time series, and the greater the complexity, the more randomized the series. Permutation entropy (PE) is a complexity measure method used to measure the amount of information contained in a time series [32]. PE can be used to detect changes in the dynamics of systems. This can be useful in detecting changes in the behavior of complex dynamical systems. The important information content associated with PE is a result of its ability to effectively distinguish between chaotic and non-chaotic signals. It is stated that PE has higher processing speeds among similar algorithms that measure complexity [33]. PE is chosen as it provides a faster and more accurate estimation of numerical sequences; therefore, PE is used to analyze the complexity of the system.

3 Numerical Results and Discussion

Numerical simulations of the system (4) are carried out using Verner's 9/8 Runge–Kutta integration method with step size $\Delta t = 0.01$ [34]. Algorithms established in the Julia code editor were implemented using the DynamicalSystems.jl library to perform the simulations [35, 36].

In this study, regular state of the system (4) which is obtained as fermionic instanton solutions [18] that are stable in a long time-scale for $\beta = 1$ with equilibrium point $(q, p) = (0.5, 0.5)$ are considered. To discriminate all possible behavior, color maps covering a large region of the SALI time (S_t) and PE of the system (4) are plotted with different initial values and parameters $f_1, f_2, \omega_1, \omega_2$. For a more detailed analysis in regions, S_t, PE and bifurcation diagrams of the system (4) are plotted by changing the

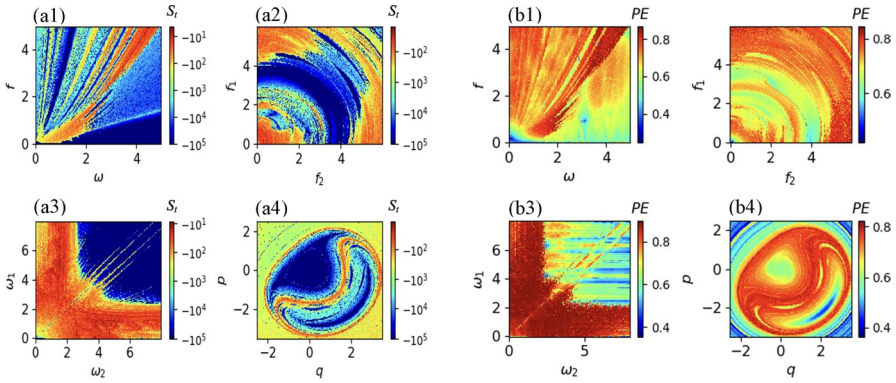

Fig. 1 Color maps of the SALI time (S_t) **(a)** and Permutation Entropy **(b)** of system (4) on the (f, ω) parameter plane with $f=f_1=f_2$ and $\omega=\omega_1=\omega_2$, where f and ω are varied from 0 to 5 for $t=10^5$ time units. The colorbars are in $\log_{10}$-scale in **(a)**

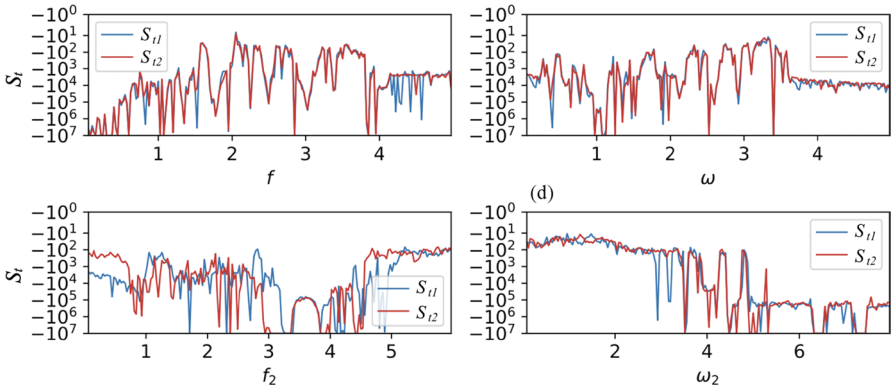

Fig. 2 Diagrams of the SALI time (S_t) of the system (4) versus parameters; f for $\omega=2.6$ (**a**), ω for f=3.0 (**b**), f_2 for $f_1=1.6$, $\omega=1.0$ (**c**) ω_2 for $\omega_1=4.0$, f=1.0 (**d**) and $t=10^7$ time units with symmetric initial values (+0.5, +0.5) (S_{t1}) (blue) and (−0.5, −0.5)(S_{t2})(red). The panels are in $\log_{10}$-scale for vertical-axes

initial values and parameter and keeping the other fixed. Considering these analyzes, samples in different states are selected. The distinction between the different behaviors of the system (4) is shown by investigating the attractors for these examples.

In panels in Fig. 1(a) blue areas denote regular states namely, SALI indices that do not become $<10^{-12}$ (threshold value) in indicated time ($t=10^5$ time units), red areas represent states of chaos namely, SALI indices that fall below $<10^{-12}$ in a short period of time and different degrees of chaotic behavior are colors between red and blue. However, it should be noted that regular orbits may become chaotic over increasing time units. Therefore, longer numerical integration times up to $t=10^7$ are performed in Fig. 2, to analyze the possible different degrees of chaos in more detail. Similarly, in Fig. 1(b), 10^5 integration time for PE, blue areas denote the lowest complexity and red areas denote the highest complexity.

Color maps in Figs. 1(a1) and (b1) show the global dynamics of the system (4) under the effect of identical two forcing terms for different values of $f=f_1=f_2$ and $\omega=\omega_1=\omega_2$ parameters. The color maps of the SALI time (S_t) and PE of the system (4) are calculated by increasing the parameters by 0.01 in the intervals $f\in(0,5]$ and $\omega\in(0,5]$ for $t=10^5$. Figures 1(a2) and (b2) demonstrate the global dynamics of the system (4) only for varying values of the f_1 and f_2. Color maps of the S_t and PE in these Figs. are plotted in the intervals $0<f_1\leq 6$ and $0<f_2\leq 6$ by increasing f_1 and f_2 by 0.01 for $\omega_1=\omega_2=1.0$ with $t=10^5$ time units. In Figs. 1(a3) and (b3) global dynamics of the system (4) is investigated with varying values of the parameters ω_1 and ω_2 for f_1 and $f_2=1.0$. Figures 1(a3) and (b3) depict color maps of the S_t and PE, plotted in the intervals $0<\omega_1\leq 8$ and $0<\omega_2\leq 8$ by increasing the parameters ω_1 and ω_2 by 0.01 with $t=10^5$ time units. Panels (a4) and (b4) in Fig. 1 demonstrate the behavior of the system (4) with changing initial values under the effect of identical two forcing terms with the parameters $f_1=f_2$ and $\omega_1=\omega_2$. In Figs. 1(a4) and (b4), the dynamic nature of the system (4) is investigated according to the initial values for parameters $f_1=f_2=3$ and $\omega_1=\omega_2=1.082$ which are determined by considering Figs. 1(a1),(b1). Color plots of the S_t and PE of the phase space of system (4) are plotted in increments of 0.01in the intervals $-2.5<q\leq 4$ and $-4<p\leq 2.5$ with $t=10^5$ time units.

Regular orbits are in blue, irregular orbits are in red, and different degrees of chaos and complexity are in intermediate colors in Fig. 1. As can be seen in Fig. 1, the forced Thirring instanton for different initial conditions and parameters have plentiful dynamical behaviors. The dynamical behavior of the system (4) is investigated in more detail by varying one parameter and keeping other fixed. Moreover, Figs. 2, 3 and 4 are plotted to examine and compare the dynamical behavior of the system with respect to the symmetric initial conditions namely, (0.5, 0.5) denoted blue and (−0.5, −0.5) denoted red.

Figure 2 demonstrates SALI time (S_t) diagrams of the system (4), calculated by increasing the parameters by 0.01 in the intervals; $f(f_1=f_2)\in(0,5]$ for $\omega(\omega_1=\omega_2)=2.6$ in panel (2a), $\omega\in(0,5]$ for $f=3.0$ in panel (2b), $f_2\in(0,6]$ for $f_1=1.6$, $\omega=1.0$ in panel (2c) and $\omega_2\in(0,8]$ for $\omega_1=4.0, f=2.6$ in panel (2d) with $t=10^7$ time units.

SALI time (S_t) indicates the time when the SALI index reaches the threshold value. Since the final integration time is determined as 10^7 time units, the S_t it takes to reach the threshold value during the time is shown in Fig. 2. It should be noted that 10^7 time units is the time when the computation is finished. If the SALI index does not reach the threshold value within this time, the time is expressed as the result.

SALI indices reaching the threshold value in a short time indicate the presence of chaos. SALI indices reaching the threshold value in a long time indicate weakly chaotic states. S_t at -10^7 indicate SALI indices that did not reach the threshold value, indicating that they are in a regular state. When looking at Fig. 2, it is seen that the system exhibits chaotic and weakly chaotic behaviors in the examined intervals, except for a few points in general. Moreover, when compared for symmetrical initial conditions, panels (a) and (b) in Fig. 2 show a great deal of similarity, but there are differences in panels (c) and (d). In this case, it shows that the amplitudes and frequencies of two forcing terms acting on us do not cause a serious change in terms of the symmetric initial conditions when they are of equal magnitude. However, it is

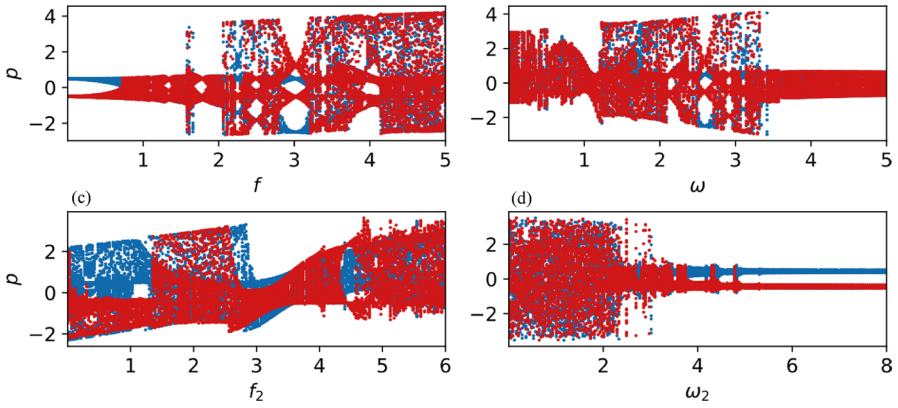

Fig. 3 Coexisting bifurcations diagrams of the system (4) obtained in the same regions of parameters with same symmetric initial values (+0.5, +0.5) (blue) and (−0.5, −0.5) (red) in Fig. 2.

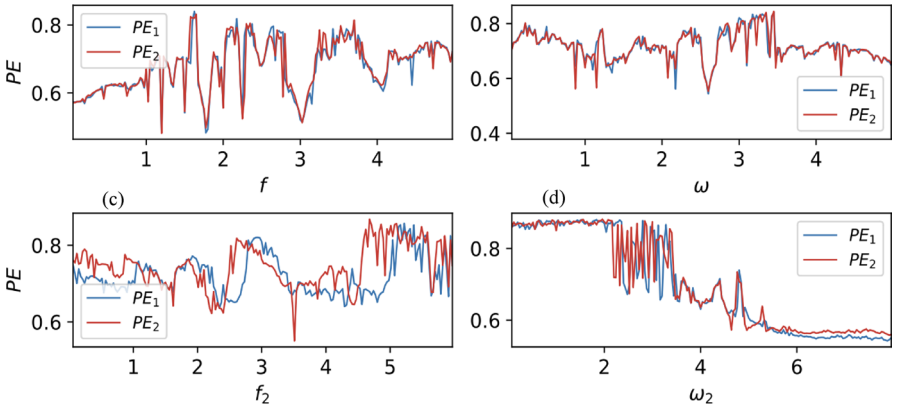

Fig. 4 Same as Figs. 2 and 3 but for PE 2 with same symmetric initial values (+0.5, +0.5) (PE_1) (blue) and (−0.5, −0.5) (PE_2)(red)

seen that panels (c) and (d) show differences in terms of frequencies and amplitudes when there are different magnitudes from each other.

All panels in Fig. 3 are plotted using the interval and same parameter and initial conditions as in Fig. 2, respectively. Figure 3 demonstrate coexisting bifurcations diagrams of the system (4) with symmetric initial values (+0.5, +0.5) (blue) and (+0.5, +0.5) (red). Considering the S_t diagrams drawn for the different cases of the system (4) in Fig. 2, it can be seen that they are mutually compatible with the bifurcation diagrams in each panel in Fig. 3.

Figure 4 shows the PE diagrams plotted for the same parameters and interval as the panels in Figs. 2 and 3 with $t=10^7$ time units. The PE value quantifies the complexity of the system, where higher values indicate greater irregularity. When Fig. 4 is examined, it is seen that the system has different complexity level in varying parameters. In addition, when compared for symmetric initial conditions, panels (a)

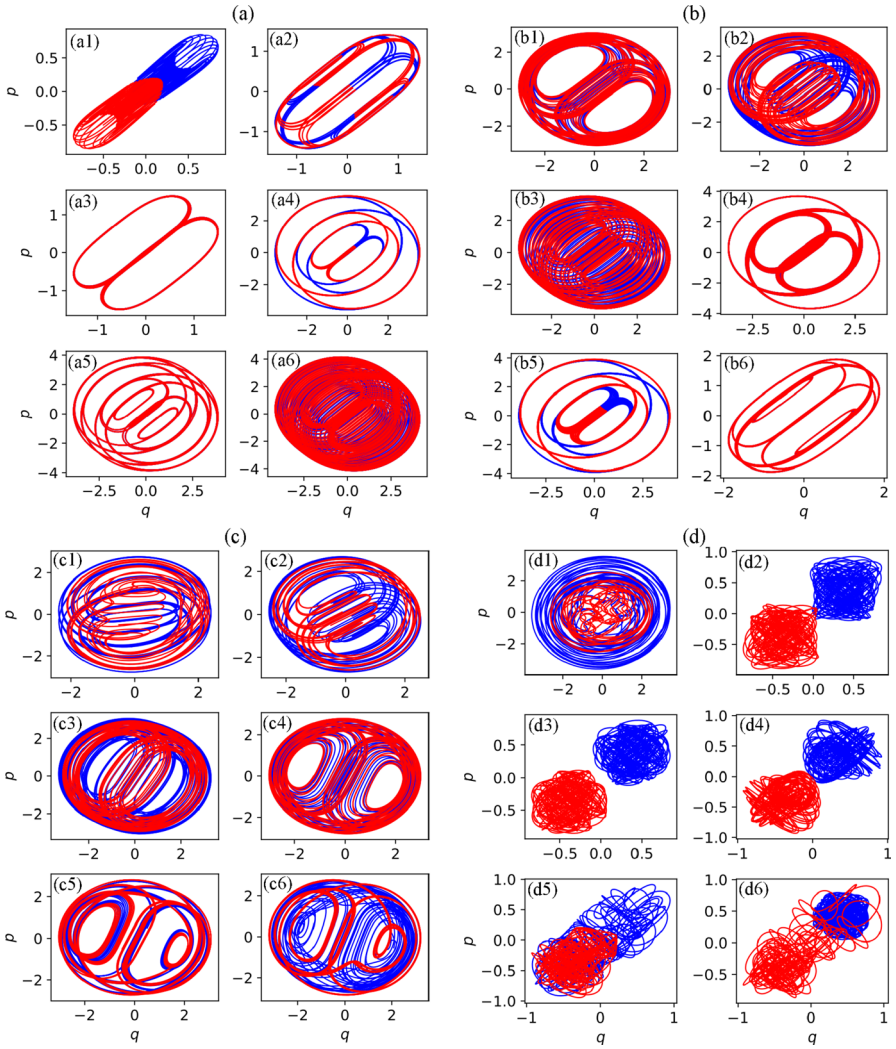

Fig. 5 Phase portraits of attractors in the system (4) with symmetric initial conditions (+0.5, +0.5) (blue) and (−0.5, −0.5) (red), for ω=2.6; when f=0.7 (**a1**), f=1.557 (**a2**), f=1.777 (**a3**), f=2.246 (**a4**), f=3.376 (**a5**) and f=4.5 (**a6**), for f=3.0; when ω=1.082 (**b1**), ω=1.713 (**b2**), ω=1.85 (**b3**), ω=2.136 (**b4**), ω=3.11 (**b5**) and ω=3.4 (**b6**), for $f_1=1.6$ and ω=1.0; when $f_2=0.22$ (**c1**), $f_2=1.14$ (**c2**), $f_2=3.22$ (**c3**), $f_2=3.6$ (**c4**), $f_2=3.76$ (**c5**) and $f_2=4.42$ (**c6**), for $\omega_1=4.0$ and f=1.0; when $\omega_2=0.38$ (**d1**), $\omega_2=3.11$ (**d2**), $\omega_2=3.4$ (**d3**), $\omega_2=4.19$ (**d4**), $\omega_2=4.343$ (**d5**) and $\omega_2=4.76$ (**d6**)

and (b) in Fig. 4 are largely similar, as are the SALI and bifurcation diagrams, but there are differences in panels (c) and (d).

Considering Figs. 2, 3 and 4, the SALI, and PE diagrams accurately demonstrate the observed bifurcation sequence when the parameters are changed. Figure 5 presents a detailed visualization of the trajectories in phase space of the system (4) for various parameter values, highlighting how the nature of the attractors changes with different combinations of the amplitudes and frequencies of the two forcing terms.

The subpanels (a1)–(a6) show how increasing the forcing amplitude f under a fixed frequency $\omega = 2.6$. Subpanels (b1)–(b6) illustrate the system's response to varying ω with fixed amplitude $f = 3.0$. Panels (c1)–(c6) and (d1)–(d6) show the effects of varying one forcing component (f_2 and ω_2, respectively) while keeping the other constant. The detailed results presented in Fig. 5(a) show that system (4) exhibit coexisting pairs symmetric attractors for $f = 0.7$ (a1), $f = 1.56$ (a2) and $f = 2.25$ (a4), coexisting pairs identical attractors for $f = 1.78$ (a3) and $f = 3.38$ (a5) and chaotic attractors for $f = 4.5$ (a6) with symmetric initial conditions $(+0.5, +0.5)$ (blue), $(-0.5, -0.5)$ (red) and $\omega = 2.6$. Panels in Fig. 5(b) demonstrate that system (4) exhibit coexisting asymmetric attractors when $\omega = 1.082$ (b1), coexisting pairs symmetric attractors when $\omega = 1.713$ (b2) and $\omega = 3.11$ (b5), coexisting pairs identical attractors when $\omega = 2.136$ (b4) and $\omega = 3.4$ (b6) and chaotic attractors when $\omega = 1.85$ (b3) with symmetric initial conditions $(+0.5, +0.5)$ (blue), $(-0.5, -0.5)$ (red) and $f = 3.0$. As seen panels (5c) and (5d) in Fig. 5, the system generally exhibits asymmetric coexisting attractors and chaotic attractors for the parameters given in the description of the Fig. 5.

Considering the Fig. 5(a) and 5(b), it is seen that two forcing terms on the system can exhibit similar behaviors in terms of the same frequency and amplitude values compared to the symmetric initial conditions. On the other hand, it can be said that they exhibit different behaviors at different frequency and amplitude values.

When the color maps and diagrams of S_t in the study are examined comparatively, it is seen that the SALI time method clearly distinguishes different degrees of chaotic regimes. In fact, S_t allows a more precise calculation by detecting exactly when the orbit starts to exhibit chaotic features. It also provides easy comparison with bifurcation diagram and PE complexity method.

4 Conclusion

The dynamical nature of fermionic instanton solutions of Thirring model via Heisenberg ansatz under two forcing terms was investigated. This approach, which extends the forced Thirring instanton with two forcing terms, aims to investigate the effects of time-periodic perturbations on fermionic instanton dynamics, with a particular focus on the emergence of chaotic behavior induced by external influences. The numerical analysis based on the SALI, bifurcation diagram and Permutation Entropy methods were used to show how chaotic behavior occurs in the system. Moreover, the chaotic nature of forced Thirring instanton was studied with diagrams and color maps of the SALI, bifurcation diagrams and PE for various of the frequency and amplitude values and initial values. Furthermore, phase portraits illustrating different types of attractors corresponding to various chaotic behavior were presented.

According to the results of this study, the fermionic instanton solutions (4), which have been shown to be stable in Ref [18]., exhibit diverse dynamical behaviors under two forcing terms according to different initial values and the frequency and amplitude values. It is seen that different types of novel chaotic attractors emerge according to different values of two forcing terms acting on fermionic instanton solutions. These results offer valuable insights into the behavior of fermionic instantons under

various conditions. It can be used to study the effects of interactions between fermions, and how these interactions can lead to new phenomena.

The SALI or $GALI_2$ method detects chaotic behaviors quickly and effectively, and the SALI indices can be distinguished between different chaotic behaviors by calculating the time to reach $< 10^{-12}$. The paper in Ref [21]. showed that it gives similar results between the LLE diagram, which is the most widely used method for detecting different degrees of chaos, and the $GALI_2$ time diagrams. In this study, it is shown that SALI time (S_t) which is practically equivalent to $GALI_2$ time, can be quickly and effectively used to compare bifurcation diagrams and the Permutation Entropy method in chaos and complexity research.

Author Contributions MA is the only contributor in the preparation of this manuscript.

Funding No funding.

Data Availability No datasets were generated or analysed during the current study.

Declarations

Competing Interests The authors declare no competing interests.

Ethics Approval and Consent to Participate Not applicable.

Consent for Publication Not applicable.

References

1. Mariño, M.: Instantons and Large N: an Introduction To Non-Perturbative Methods in Quantum Field Theory. Cambridge University Press, Cambridge (2015)
2. Belavin, A.A., Polyakof, A.M., Schwartz, A.S., Tyupkin, Y.S.: Pseudoparticle solutions of Yang–Mills equations. Phys. Lett. B **59**, 85–87 (1975)
3. Coleman, S.R.: The uses of instantons. Subnucl. Ser. **15**, 805 (1979)
4. Hooft, G.: T: Symmetry breaking through Bell-Jackiw anomalies. Phys. Rev. Lett. **37**, 8–11 (1976)
5. Affleck, I., Harvey, J., Witten, E.: Instantons and (Super-) symmetry breaking in (2+1) dimensions. Nucl. Phys. B. **206**(3), 413–439 (1982). https://www.sciencedirect.com/science/article/abs/pii/0550321382902772?via%3Dihub
6. Gross, D.J., Neveu, A.: Dynamical symmetry breaking in asymptotically free field theories. Phys. Rev. D. **10**, 3235–3253 (1974)

7. Fubuni, S.: A new approach to conformal invariant field theories. II Nuovo Cim A. **34**, 521–554 (1976)
8. Alexandre, J., Polonyi, J.: Symmetry restoration, tunneling, and the null energy condition. Phys. Rev. D **106**, 065008 (2022)
9. Frishman, Y., Sonnenschein, J.: Non-Perturbative Field Theory: from Two-Dimensional Conformal Field Theory To QCD in Four Dimensions. Cambridge University Press, Cambridge (2010)
10. Rischke, D.H.: The quark–gluon plasma in equilibrium. Part. Nuclear Phys. **52**, 197–296 (2004)
11. Coley, A.A., Ellis, G.F.R.: Theoretical cosmology. Classical and Quantum Gravity **37**, 013001 (2020)
12. Barrientos, J., Cisterna, A., Corral, C., Oyarzo, M.: Gravitational instantons with conformally coupled scalar fields. J. High Energ. Phys. 110 (2022)
13. Thirring, W.: A Soluble Relativistic Field Theory. Annals of Physics (1),(1958). https://doi.org/10.1016/0003-4916(58)90015-0
14. Wetterich, C.: Fermionic quantum field theories as probabilistic cellular automata. Phys. Rev. D **105**, 074502 (2021)
15. Sugiura, M.: Fermion mass generation in the D-dimensional thirring model as a gauge theory. Prog Theor. Phys. **97**, 311–326 (1997)
16. Campa, A., Casetti, L., Latella, I., Pérez-Madrid, A., Ruffo, S.: Phase transitions in Thirring's model. J. Stat. Mech. 073205 (2016)
17. Akdeniz, K.G., Smailagic´, A.: Classical solutions for fermionic models. Il Nuovo Cimento A. **51**, 345–357 (1979)
18. Canbaz, B., Onem, C., Aydogmus, F., Akdeniz, K.G.: From Heisenberg ansatz to attractor of thirring instanton. Chaos Solitons Fractals. **45**, 188–191 (2012)
19. Aydogmus, F., Canbaz, B., Onem, C., Akdeniz, K.G.: The behaviours of Gursey instantons in phase space. Acta Phys. Pol., B. **44**, 1837–1845 (2013)
20. Yılmaz, N., Canbaz, B., Akıllı, M., Önem, C.: Study of the stability of the fermionic instanton solutions by the scale index method. Phys. Lett. A. **382**, 2118–2121 (2018)
21. Canbaz, B.: Chaos classification in forced fermionic instanton solutions by the generalized alignment index (GALI) and the largest Lyapunov exponent. Chaos, Solitons & Fractals **164**, 112685 (2022)
22. Akıllı, M., Yılmaz, N.: Entropy of the quantum fluctuations of fermionic instantons in the universe. Mod. Phys. Lett. A **37**(16), 2250101 (2022)
23. Yılmaz, N., Akıllı, M., Akdeniz, K.G.: Thirring universe model. Phys. Scr. **99**(10), 105044 (2024)
24. Devaney, R.L.: An Introduction To Chaotic Dynamical Systems. CRC (2021)
25. Lorenz, E.: The Essence of Chaos. University of Washington (1993)
26. Skokos, C.: Alignment indices: A new, simple method for determining the ordered or chaotic nature of orbits. J. Phys. A: Math. Gen. **34**, 10029–10043 (2001)
27. Skokos, C., Antonopoulos, C., Bountis, T.C., Vrahatis, M.N.: Detecting order and chaos in hamiltonian systems by the SALI method. J. Phys. A Math. Gen **37**, 6269–6284 (2004)
28. Skokos, C., Bountis, T., Antonopoulos, C.: Geometrical properties of local dynamics in hamiltonian systems: The generalized alignment index (GALI) method. Physica D: Nonlinear Phenomena **231**, 30–54 (2007)
29. Hillebrand, M., Zimper, S., Ngapasare, A., Katsanikas, M., Wiggins, S., Skokos, C.: Quantifying chaos using lagrangian descriptors. Chaos **32**, 123122 (2022)
30. Senyange, B., Skokos, C.: Identifying localized and spreading chaos in nonlinear disordered lattices by the generalized alignment index (GALI) method. Physica D: Nonlinear Phenomena **432**, 133154 (2022)
31. Ngapasare, A., Theocharis, G., Richoux, O., Skokos, C., Achilleos, V.: Wave-packet spreading in disordered soft architected structures. Chaos **32**, 053116 (2022)
32. Bandt, C., Pompe, B.: Permutation entropy: A natural complexity measure for time series. Phys. Rev. Lett. **88**, 174102 (2022)
33. Liu, H., He, P., Li, G., Xu, X., Zhong, H.: Multi-directional annular multi-wing chaotic system based on Julia fractals. Chaos Solitons Fractals **165**(1), 112799 (2022)
34. Verner, J.H.: Numerically optimal Runge–Kutta pairs with interpolants. Numer. Algor. **53**, 383–396 (2010)
35. Rackauckas, C., Nie, Q.: DifferentialEquations.jl—A performant and feature-rich ecosystem for solving differential equations in Julia. J. Open. Res. Softw. **5**, 15 (2017)
36. Datseris, G.: DynamicalSystems.jl: A Julia software library for chaos and non- linear dynamics. J. Open. Source Softw. **3**, 598 (2018)